This is an open access article published under an ACS AuthorChoice License, which permits copying and redistribution of the article or any adaptations for non-commercial purposes.

ACS OMEGA

Article

http://pubs.acs.org/journal/acsodf

NiO_x Hole Transport Layer for Perovskite Solar Cells with Improved Stability and Reproducibility

Md. Bodiul Islam,[†,‡,§] Masatoshi Yanagida,[†] Yasuhiro Shirai,[*,†] Yoichi Nabetani,[‡] and Kenjiro Miyano[†]

[†]Global Research Center for Environment and Energy based on Nanomaterials Science (GREEN), National Institute for Materials Science, 1-1 Namiki, Tsukuba, Ibaraki 305-0044, Japan

[‡]Interdisciplinary Graduate School of Medicine and Engineering, University of Yamanashi, 4-3-11 Takeda, Kofu, Yamanashi 400-8511, Japan

[§]Department of Glass and Ceramic Engineering, Rajshahi University of Engineering & Technology, Rajshahi 6204, Bangladesh

Supporting Information

ABSTRACT: In this study, highly stable, low-temperature-processed planar lead halide perovskite ($MAPbI_{3-x}Cl_x$) solar cells with NiO_x interfaces have been developed. Our solar cells maintain over 85% of the initial efficiency for more than 670 h, at the maximum power point tracking (MPPT) under 1 sun illumination (no UV-light filtering) at 30 °C, and over 73% of the initial efficiency for more than 1000 h, at the accelerating aging test (85 °C) under the same MPPT condition. Storing the encapsulated devices at 85 °C in dark over 1000 h revealed no performance degradation. The key factor for the prolonged lifetime of the devices was the sputter-deposited polycrystalline NiO_x hole transport layer (HTL). We observed that the properties of NiO_x are dependent on its composition. At a higher Ni^{3+}/Ni^{2+} ratio, the conductivity of NiO_x is higher, but at the expense of optical transmittance. We obtained the highest power conversion efficiency of 15.2% at the optimized NiO_x condition. The sputtered NiO_x films were used to fabricate solar cells without annealing or any other treatments. The device stability enhanced significantly compared to that of the devices with PEDOT:PSS HTL. We clearly demonstrated that the illumination-induced degradation depends heavily on the nature of the HTL in the inverted perovskite solar cells (PVSCs). The sputtered NiO_x HTL can be a good candidate to solve stability problems in the lead halide PVSCs.

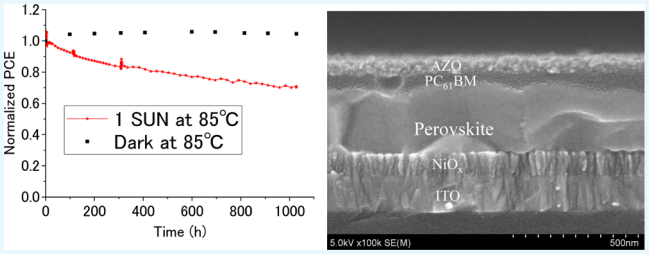

INTRODUCTION

After the invention of organic−inorganic hybrid perovskite solar cell (PVSC) with 3.81% power conversion efficiency (PCE) by Kojima et al.,[1] it has attracted much attention because of its low cost and easy fabrication. Within a very short period of time, PVSCs have achieved a rapid development and the PCE exceeded 20%, comparable to those of the conventional silicon solar cells.[2,3] There have also been a growing interest in the development of low-temperature-processed PVSCs with inverted device structures because of their lower fabrication cost and new solar cell applications with their light weight and flexibility. However, it is still a great challenge to fabricate PVSCs with long lifetime using low-temperature processes for successful commercialization. Although the impressive high efficiency of PVSCs stands up to those of other existing PV technologies with >20% efficiency, the rapid degradation phenomena broadly observed for PVSCs overshadow the future of this PV technology.[4] The literature concerning the real performance of the PVSCs in long-term operations is still limited, and many studies on the perovskite stabilities focus on the stored lifetime (shelf-life).[5,6] As far as we know, there have been only a few reports on the stability of the operating conditions of PVSCs under light.[7−12] The purpose of this study is to examine the effect of an interface layer on the long-term operation of low-temperature-processed PVSCs under real working conditions, with maximum power point tracking (MPPT) under 1 sun (AM1.5G) illumination (no UV-light filtering) and in the accelerated aging at 85 °C under the same MPPT condition.

One of the possible reasons for the instability of the PVSCs is the instability and/or adverse effects of the organic hole transport layers (HTLs),[13−16] and we set out to develop an ideal HTL that has a suitable energy level with perovskite, high optical transparency in the visible range, and high stability and supports the fabrication of thick and high-quality perovskite films. Because of their large band gap (~3.6 eV), deep valance band edge (~5.4 eV), ease of controlling composition, and low cost with superior thermal and chemical stabilities, NiO derivatives were identified to achieve our goal. In fact, NiO-based HTLs have been used for the fabrication of inverted and other type of PVSCs, and the stability issue often became a focus in studies concerning them (Table S1).[7,14,16−36] In this study, we demonstrate inverted planar PVSCs on the basis of the sputter-deposited polycrystalline NiO_x hole transport

Received: April 30, 2017
Accepted: May 11, 2017
Published: May 24, 2017

© 2017 American Chemical Society

DOI: 10.1021/acsomega.7b00538
ACS Omega 2017, 2, 2291−2299

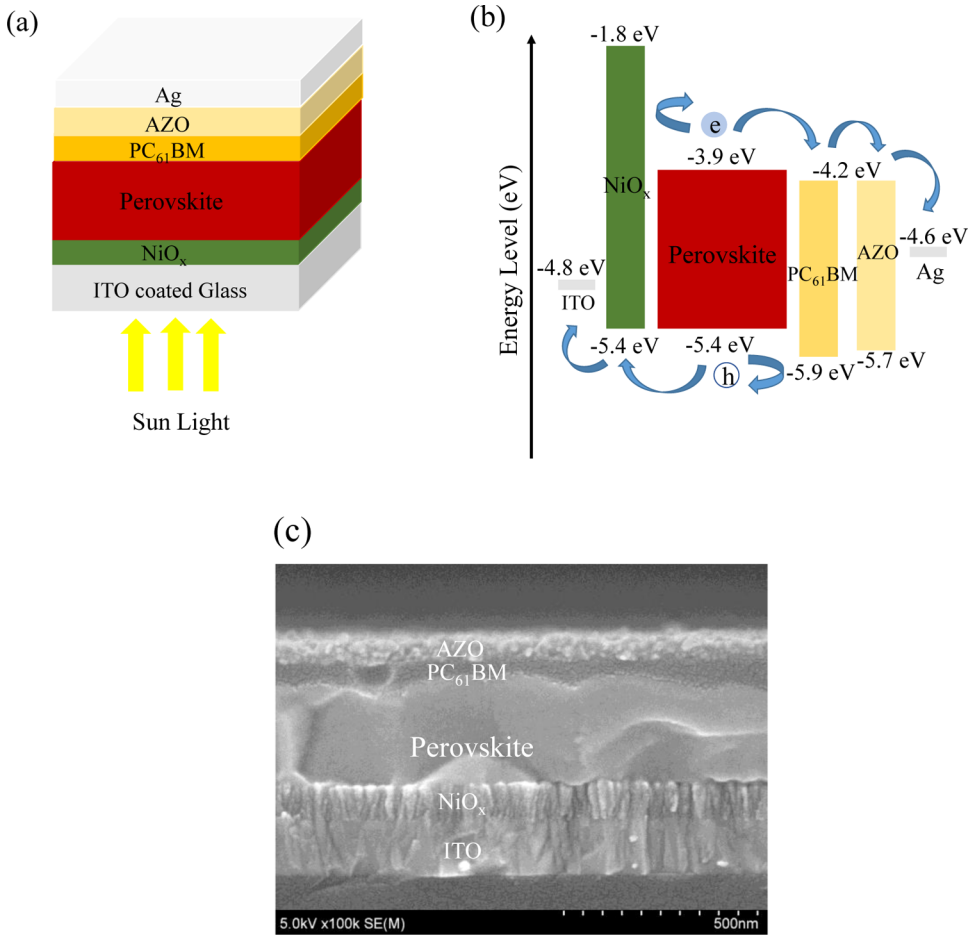

Figure 1. (a) Device structure consisting of ITO-coated glass/NiO_x/perovskite ($CH_3NH_3PbI_{3-x}Cl_x$)/$PC_{61}BM$/AZO/Ag and (b) the corresponding energy band diagram and (c) cross-sectional SEM image.

material. We prepared compact and homogeneous NiO_x films on indium tin oxide (ITO)-coated glass by radio frequency (rf) magnetron sputtering, allowing us to control the oxygen composition and thickness, with high reproducibility.[20] We revealed in detail the effect of NiO_x composition and thickness (from 20 to 250 nm) on the device performance and showed that fine-tuning of the composition (Ni^{3+}/Ni^{2+} ratio) and thickness resulted in high-performance PVSCs with over 15% efficiency and unprecedented stability for low-temperature-processed $MAPbI_{3-x}Cl_x$ devices. We also compared the stabilities of the NiO_x-based devices and the PEDOT:PSS-based devices under continuous illumination from a class AAA solar simulator and MPPT condition. Surprisingly, the NiO_x-based devices maintained about 73% of the initial efficiency after 1000 h of continuous operation under the 85 °C accelerated aging condition, whereas the PEDOT:PSS-based devices maintained only <20% of the initial efficiency at 30 °C within 400 h of operation. We clearly demonstrated that the illumination-induced degradation significantly depends on the nature of the HTL in the inverted PVSCs. The sputtered NiO_x HTL can be a good candidate to solve stability problems in the low-temperature-processed lead halide PVSCs.

RESULTS AND DISCUSSION

The device structure of our PVSC is shown in Figure 1a. This inverted structure consists of ITO-coated glass/NiO_x/perovskite ($CH_3NH_3PbI_{3-x}Cl_x$)/$PC_{61}BM$/aluminum-doped zinc oxide (AZO)/Ag, where the NiO_x is the HTL (or electron-blocking layer) and $PC_{61}BM$/AZO is the electron transport layer. The corresponding band diagram and energy levels are shown in Figure 1b. The scanning electron microscopy (SEM) cross section of the device is illustrated in Figure 1c. Sealing glass was used to encapsulate the device, to protect it from moisture and oxygen.

Properties of NiO_x Thin Films. NiO_x films were fabricated at different Ar pressures of the deposition chamber; the optical and electrical properties of the resulting NiO_x films depend on the deposition conditions, and it was found that at lower pressure, because of Ni vacancy/excess oxygen in the films, they became blackish (Figure S1). This observation parallels to that of the previous study with compact NiO_x electron-blocking layers prepared by sputtering.[20] The oxygen content of the black form was slightly greater than that of its green counterpart.[37] The defect of NiO films is due to the interstitial oxygen or Ni^{2+} vacancy that occurs as a result of the creation of Ni^{3+} ions. For each Ni^{2+} vacancy (Ni_v), two Ni^{2+} ions must be converted to Ni^{3+} to preserve the overall charge neutrality in the crystal. This ensures excess oxygen compared to the number of nickel ions in the crystal. Finally, the creation of defects in NiO_x crystals can be expressed with the following equation

$$2NiO \rightarrow 2Ni^{3+} + Ni_v + 2O^{2-}$$

DOI: 10.1021/acsomega.7b00538
ACS Omega 2017, 2, 2291−2299

Now, if an electron moves from a Ni^{2+} site to a Ni^{3+} site, it is like the movement of a hole in the opposite direction through the Ni^{2+} sites. These holes contribute to the electrical conductivity of undoped NiO_x crystals. Therefore, NiO_x with excess oxygen is a p-type semiconductor.[38]

To analyze the Ni^{3+}/Ni^{2+} ratio of the sputtered NiO_x thin films, they were characterized by X-ray photoelectron spectroscopy (XPS). As shown in Figure 2, the peak at 860.8 eV is

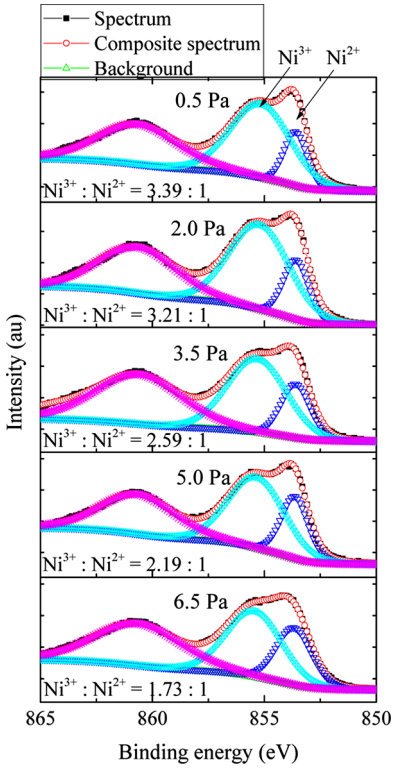

Figure 2. XPS spectra representing the Ni $^2p_{3/2}$ peak with deconvolution of Ni^{3+} and Ni^{2+} peaks of NiO_x films prepared at 0.5, 2.0, 3.5, 5.0, and 6.5 Pa Ar pressures.

due to the shake-up process of the NiO structure, the peak at 853.8 eV indicates Ni^{2+} ion, and the peak at 855.5 eV indicates Ni^{3+} ion.[23] The compositions of Ni^{2+} and Ni^{3+} in the crystals were determined by calculating the integral area of the fitting curve of the XPS spectra, and the Ni^{3+}/Ni^{2+} ratio of NiO_x films is shown in Figure 3. It is evident from the figure that the Ni^{3+}/Ni^{2+} ratio decreased with increasing pressure.

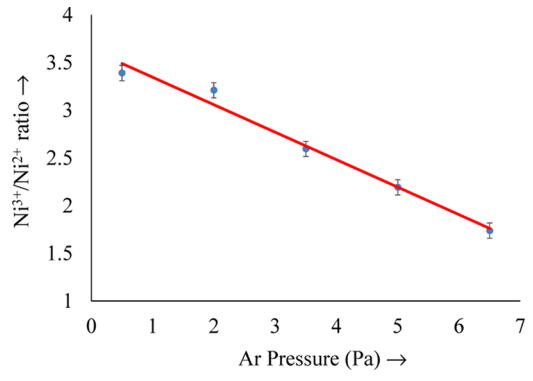

Figure 3. Composition of NiO_x films at different Ar pressures.

The films prepared by sputtering methods are polycrystalline in nature and have cubic structure, as shown in Figure 4. At

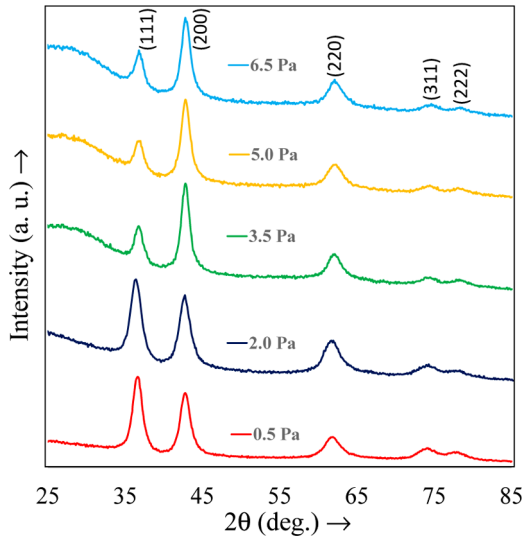

Figure 4. XRD patterns of the NiO_x films at different Ar pressures.

lower pressure, the (111) peak is dominating, and with increasing pressure, (200) peak becomes dominating. Broader X-ray diffraction (XRD) peaks indicate smaller crystals of the fabricated films. Furthermore, we studied the surface morphology of NiO_x films by SEM, as shown in Figure 5. The SEM images demonstrate small grains of NiO_x films, and the grain size is dependent on the thickness of the films. At a lower thickness (~20 nm), the grain size is quite small; however, with increasing thickness (up to 250 nm), the grain size gradually increases. The Ar pressure in the sputtering chamber has little effect on the grain size (Figure S2), and with increasing Ar pressure, the grain size increases. With increasing Ar pressure in the sputtering chamber, the transmittance of the prepared films also increases, as shown in Figure 6. The films prepared at 0.5 Pa have a lower transmittance of 60% at the 550 nm wavelength of the visible range of the spectrum, whereas the films prepared at or above 3.5 Pa show more than 80% transmittance at the 550 nm wavelength of the spectrum. It is notable that the difference of transmittance between the films prepared at 0.5 and 3.5 Pa is very large (~20%), whereas the effect is very little (<5%) for the films prepared at 3.5−6.5 Pa. Because of increasing Ni vacancy/excess oxygen, the films became blackish and their transmittance decreased at lower Ar pressure.

Figure 6 also compares the transmittances of the fabricated NiO_x films at different thicknesses. It is evident from the figure that transmittance declines with increasing thickness, as expected, and the only exception is at the 150 nm thickness, where the transmittance is higher than that at the 70 nm thickness. The reason may be the large grain size, as shown in Figure 5, which might reduce the light scattering by the grain boundary. The films prepared at 0.5 and 2.0 Pa have resistivities of 3.28×10^2 and 2.92×10^3 Ω·cm, respectively. However, the films prepared at the pressure range of 3.5−6.5 Pa have very high resistivities, which we could not measure using our linear four-probe system. The low resistivity of the films prepared at lower pressure possibly indicated the increased Ni vacancy/excess oxygen in the crystals, which act as the hole and contribute to the electrical conductivity. This effect is quite

DOI: 10.1021/acsomega.7b00538
ACS Omega 2017, 2, 2291−2299

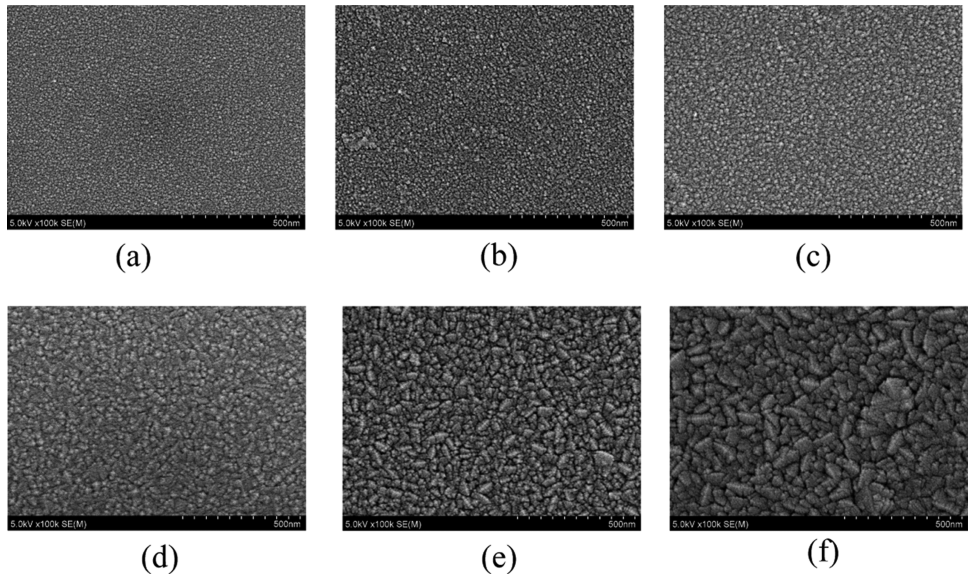

Figure 5. SEM images of NiO_x films fabricated at 3.5 Pa with different thicknesses of (a) 20 nm, (b) 50 nm, (c) 70 nm, (d) 100 nm, (e) 150 nm, and (f) 250 nm.

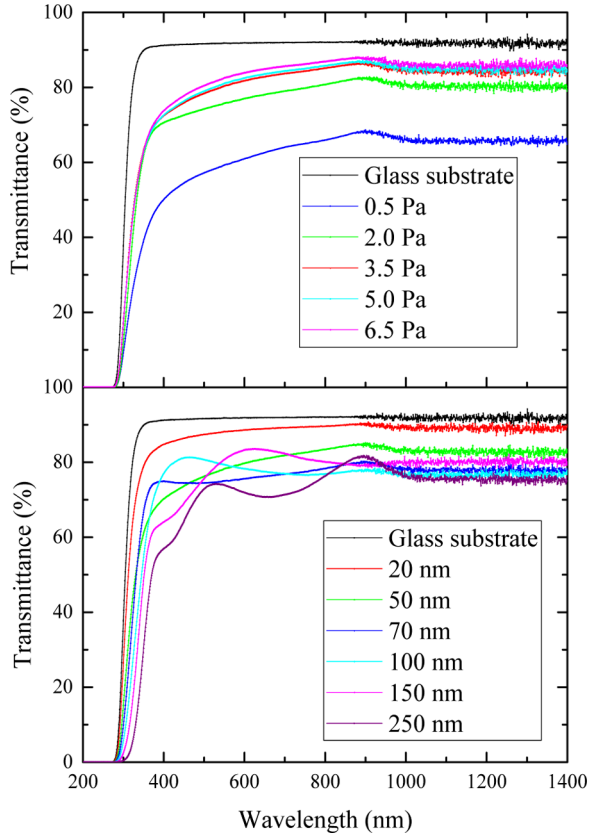

Figure 6. Transmission spectra of NiO_x films on glass substrate at different Ar pressures (film thickness: 60−70 nm for 0.5−3.5 Pa and ∼40 nm for 5.0−6.5 Pa) and at different thicknesses at an Ar pressure of 3.5 Pa.

consistent with the XPS and XRD results. The resistivity values of the (200)-orientated NiO_x films are higher than those of the (111)-orientated films.[39]

Device Performances. We revealed the dependence of device performances on the Ar pressure during sputter deposition of NiO_x, and the results are summarized in Table 1 and Figure 7. It is observed that with increasing Ar pressure up to 3.5 Pa, the device performance enhanced and beyond that pressure, it declined (Figure 7a). This phenomenon can be explained with the optical and electrical properties of the sputtered NiO_x thin films. As shown in Figure 6, at lower pressure, the NiO_x thin films absorbed some part of the incident sunlight. At higher pressure, although the transmittance is better, higher resistance of the films reduces the device performance, as seen from the increased series resistance (R_s) for 5.0 and 6.5 Pa. Therefore, we selected the devices with NiO_x HTL prepared at 3.5 Pa Ar pressure for further study of thickness-dependent device performance, and the results are summarized in Table 2.

It was found that when the NiO_x layer was too thin (e.g., 20 nm), the devices showed lower PCE. The very thin film may be not sufficient to block the photogenerated electrons because of the insufficient coverage of the ITO film with the NiO_x layer, which in turn decreases the FF.[22,29] In fact, the improved FF values with increasing thickness were observed possibly due to the elimination of pinholes. However, with a very thick NiO_x HTL, the FF was satisfactory, but the PCE was again low. With higher thickness, the transmittance decreased, with a small deviation at 150 nm thickness. From Figure 7b, we can see that with higher thickness, the EQE of the devices decreased significantly at lower wavelength, which reduces their short-circuit current density (J_{sc}). Devices with a NiO_x HTL thickness of 70 ± 3 nm showed the best performance (Figure 8). Although the hysteresis behaviors of the PVSCs are an important issue, which is frequently observed and reported in the literature,[40] our NiO_x devices showed almost no hysteresis behaviors. The devices showed a good reproducibility with a limited deviation of PCE, as shown in Figure 9. Histograms of solar cell efficiencies were collected from 32 cells with NiO_x HTL of thickness 70 ± 3 nm prepared at 3.5 Pa Ar pressure.

No significant performance degradation was observed for encapsulated devices with NiO_x HTL stored at ambient temperature under dark condition for 5 months and 85 °C for 1000 h. The significant improvement of the stability over previous NiO_x-based devices (Table S1) was achieved possibly due to the synergy of the NiO_x HTL, with the high

DOI: 10.1021/acsomega.7b00538
ACS Omega 2017, 2, 2291−2299

Table 1. Performance of the Devices with Different Ar Pressures of the Deposition Chamber during Sputter Deposition of NiO_x[a]

Ar pressure (Pa)	η (%)	J_{sc} (mA/cm^2)	V_{oc} (V)	fill factor (FF)	R_s (Ω·cm^2)	R_{sh} (Ω·cm^2) × 10^3
0.5	11.02 ± 0.46	17.67 ± 0.71	0.97 ± 0.01	0.63 ± 0.03	5.01 ± 0.58	2.07 ± 0.19
2.0	12.21 ± 0.58	18.70 ± 0.83	0.98 ± 0.01	0.63 ± 0.02	5.16 ± 0.47	2.35 ± 0.72
3.5	14.76 ± 0.39	19.86 ± 0.85	1.01 ± 0.02	0.68 ± 0.02	5.41 ± 0.62	3.25 ± 0.33
5.0	13.61 ± 0.61	19.79 ± 0.69	0.98 ± 0.01	0.66 ± 0.03	8.85 ± 0.83	2.30 ± 0.46
6.5	12.09 ± 0.57	18.88 ± 0.48	0.98 ± 0.01	0.65 ± 0.04	8.74 ± 0.92	1.23 ± 0.57

[a]Data collected from at least 12 cells for each condition (NiO_x film thickness: 60−70 nm for 0.5−3.5 Pa and ∼40 nm for 5.0−6.5 Pa).

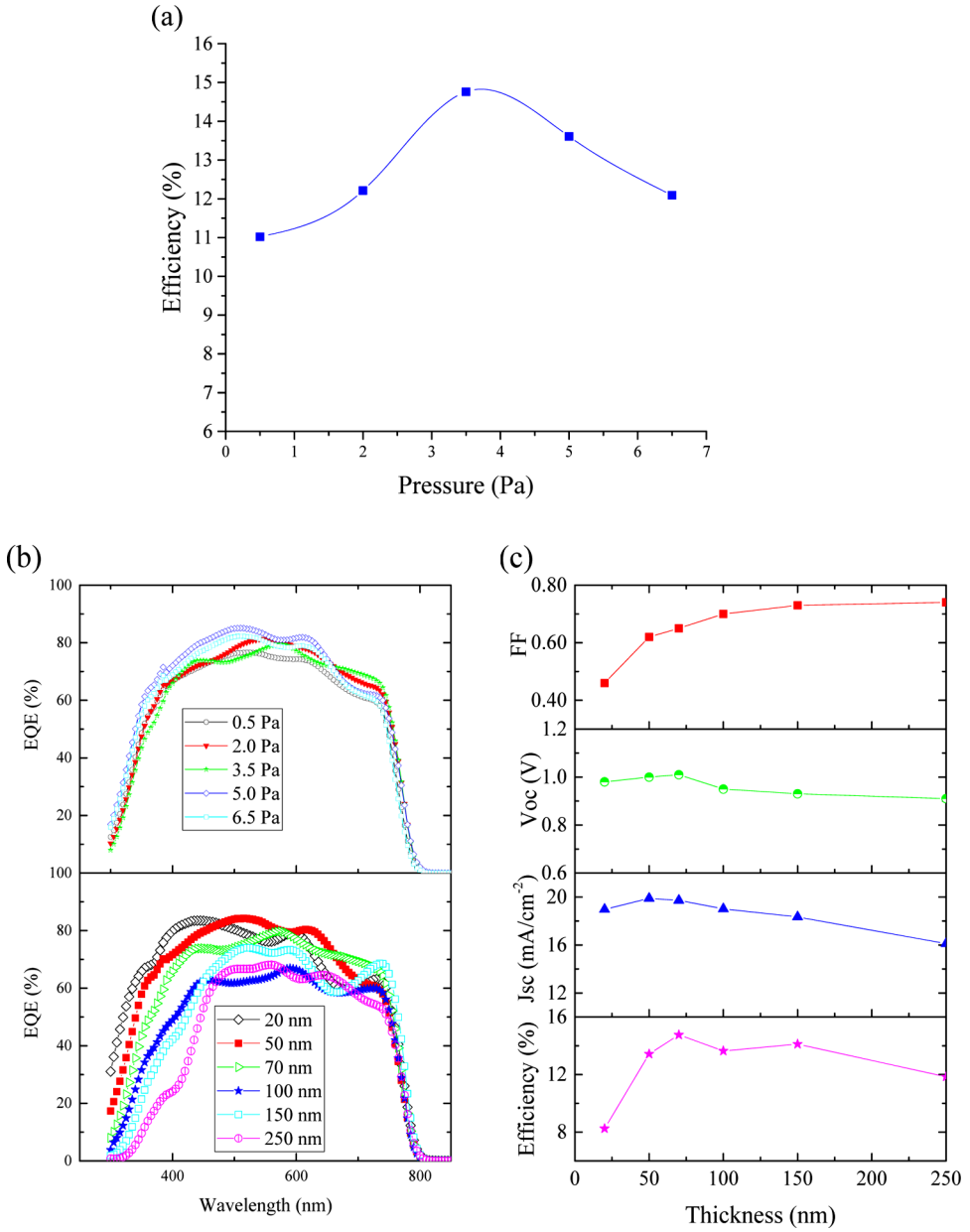

Figure 7. Device performances. (a) Ar-pressure-dependent PCE, (b) external quantum efficiency (EQE) of the devices with NiO_x HTL prepared at different Ar pressures and thicknesses, (c) PCE, J_{sc}, V_{oc}, and FF depending on NiO_x HTL thicknesses.

optoelectronic quality of the MACl-treated perovskite layer.[41] We also observed that the PCE and open-circuit voltage (V_{oc}) gradually increase with time at ambient temperature and under dark condition. The improvement can be explained by the ion migration and chemical doping of the PCBM layer by iodide.[8,42] On the other hand, under continuous 1 sun illumination (no UV-light filtering) and MPPT condition at 30 °C, the performance first degraded gradually and then the degradation rate decreased; it eventually reached 87% of the initial efficiency after 670 h of operation, as shown in Figure 10a. The PEDOT:PSS-based devices degrade rapidly, and within 400 h, they retain only <20% of the initial PCE, possibly

DOI: 10.1021/acsomega.7b00538
ACS Omega 2017, 2, 2291−2299

Table 2. Performance of the Devices with Different Thicknesses of NiO_x Prepared at 3.5 Pa[a]

NiO_x thickness (nm)	η (%)	J_{sc} (mA/cm^2)	V_{oc} (V)	FF	R_s (Ω·cm^2)	R_{sh} (Ω·cm^2) × 10^3
20 ± 2	8.25 ± 0.41	18.47 ± 0.23	0.98 ± 0.01	0.46 ± 0.11	21.48 ± 1.31	0.86 ± 0.15
50 ± 2	13.43 ± 0.56	19.89 ± 0.65	1.00 ± 0.01	0.62 ± 0.02	5.07 ± 0.45	1.47 ± 0.38
70 ± 3	14.76 ± 0.39	19.86 ± 0.85	1.01 ± 0.02	0.68 ± 0.02	5.41 ± 0.62	3.25 ± 0.33
100 ± 5	13.64 ± 0.67	19.01 ± 0.41	0.95 ± 0.01	0.69 ± 0.01	5.82 ± 0.33	3.05 ± 0.46
150 ± 5	14.12 ± 0.35	18.74 ± 0.64	0.93 ± 0.02	0.73 ± 0.01	5.35 ± 0.52	2.83 ± 0.63
250 ± 7	11.85 ± 0.58	16.11 ± 0.72	0.90 ± 0.02	0.74 ± 0.01	5.80 ± 0.61	2.76 ± 0.29

[a]Data collected from at least 12 cells for each thickness.

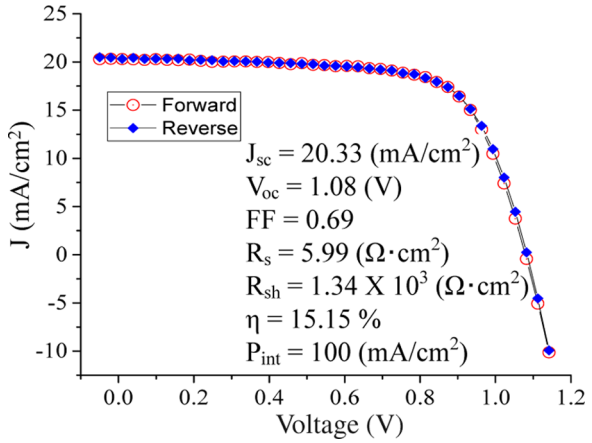

Figure 8. J–V curve of the best device with NiO_x HTL (3.5 Pa, 70 nm) under 1 sun condition measured at forward scan (−0.05 → 1.2 V; step, 0.02 V; delay time, 200 ms) and reverse scan (1.2 → −0.05 V; step, 0.02 V; delay time, 200 ms).

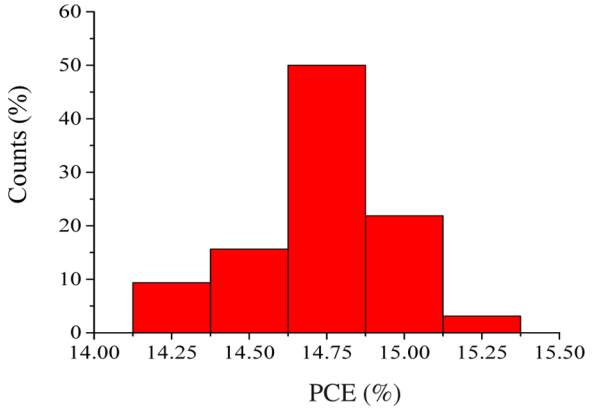

Figure 9. PCE distribution histogram of devices with NiO_x HTL prepared at 3.5 Pa.

due to the chemical nature of the PEDOT:PSS layer.[13−16] The lifetime of solar cells may be defined as the operation time until the output of the device has fallen below a certain level, that is, 70% of nominal efficiency for more than 40 years was expected from some commercial Si solar cells, and it often requires accelerated aging conditions to predict their lifetime in a reasonable testing time. In fact, the NiO_x-based devices showed surprisingly high stability and it would require significant testing time to observe degradation at 30 °C (Figure 10a). Thus, we decided to accelerate the aging by increasing the testing temperature up to 85 °C (Figure 10b). The degradation rate was indeed increased compared to that of the 30 °C testing, and the initial 14% efficiency at room temperature reduced to about 13% because of the negative-efficiency temperature coefficient of the perovskite devices.[8] Further continuation of the high-temperature testing induced significant efficiency drop from 13.0% to below 9.5%, which corresponds to 73% of the initial efficiency after 1000 h. According to the definition of the acceleration factor, K, under the assumption of an Arrhenius model, defined by the equation[43]

$$K = \exp\left[\frac{E_a}{k_B}\left(\frac{1}{T_{high}} - \frac{1}{T_{low}}\right)\right] \quad (1)$$

where E_a is the activation energy for the degradation processes in electron volts (eV), k_B is the Boltzman constant, and two testing temperatures (T_{high} = 85 °C and T_{low} = 25 °C), the result of the accelerated testing suggested that the NiO_x-based devices would operate over 7000 h (K = 7) at room temperature (T_{low} = 25 °C) before the output falls below 73% of the initial efficiency, if the activation energy (E_a) for a degradation path of these devices was 0.3 eV, which is a lower-end value estimated for a polymer solar cell.[43] In the similar manner, the device would operate over 3000 h (K = 3) at 50 °C (Figure S3), which is a typical working condition of a solar cell operating on the roof. As shown in Figure S3, the predicted lifetime based on the acceleration factor (eq 1) of the solar cells strongly relies on the activation energy (E_a); thus, accelerated aging tests at several different temperature conditions will be necessary for more conclusive discussions in future stability studies.

CONCLUSIONS

In summary, we have successfully developed efficient and hysteresis-free inverted planar lead halide PVSCs with improved stability and reproducibility using NiO_x HTLs. The NiO_x layers were prepared by rf magnetron sputtering without postdeposition annealing. Ni^{3+}/Ni^{2+} ratio in the NiO_x film not higher than ∼3 with 70 ± 3 nm thickness showed superior quality as an HTL. The synergy of the NiO_x HTL with the high optoelectronic quality of the MACl-treated perovskite layer[41] resulted in no performance degradation at 85 °C in dark. More importantly, although it was found that these encapsulated devices showed no degradation under dark condition at 85 °C over 1000 h, they still degraded under continuous 1 sun illumination at 30 and 85 °C and under MPPT operation. Nevertheless, our results demonstrated that NiO_x as HTL is a good candidate to solve stability problems in the low-temperature-processed inverted PVSCs. Further investigation is necessary to improve the solar cell performance under continuous illumination for commercial applications.

METHODS

NiO_x Film Deposition. The NiO_x thin films were prepared on the commercially available precleaned and prepatterned

DOI: 10.1021/acsomega.7b00538
ACS Omega 2017, 2, 2291−2299

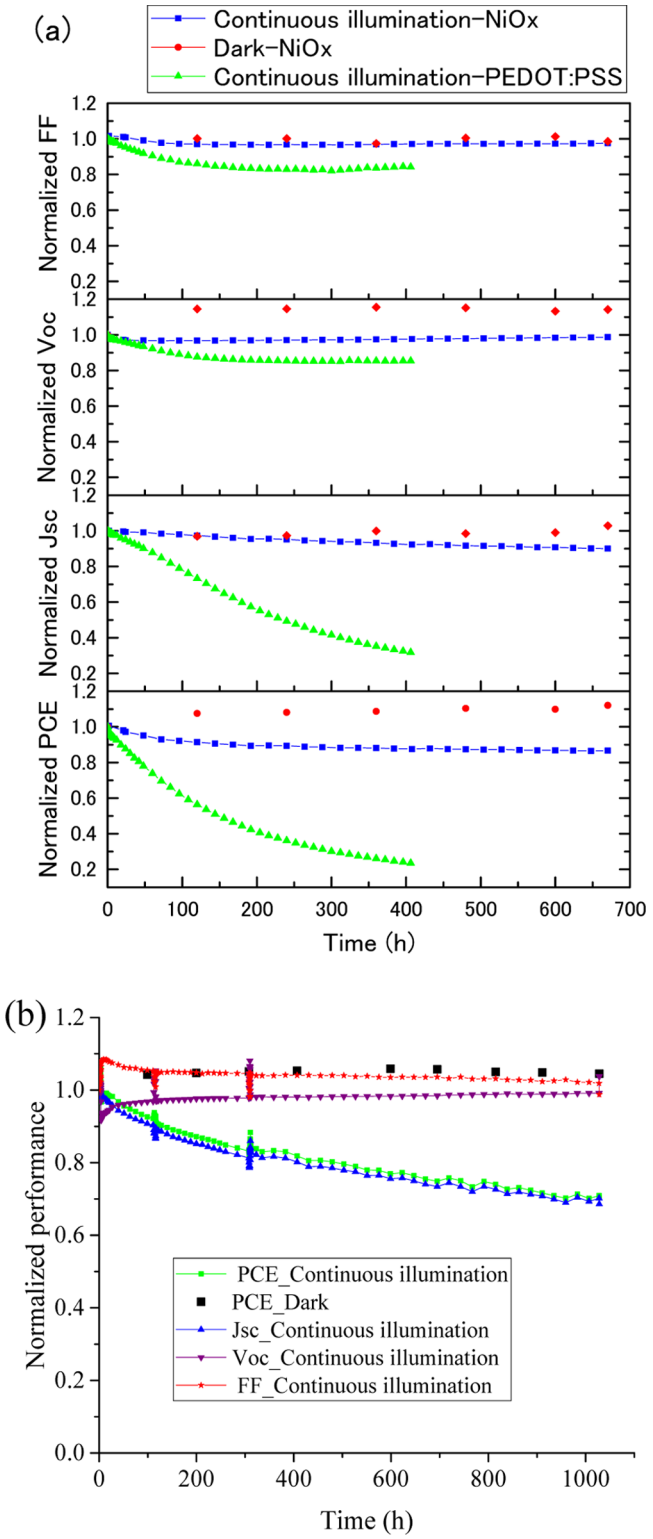

Figure 10. (a) Stability of the encapsulated device at 30 °C (~50% RH) under ambient and dark condition and under MPPT condition (1 sun) (the device was kept under MPPT condition between the periodical $J-V$ measurements). (b) Accelerated aging test at 85 °C (~5% RH) in dark and under MPPT condition (the device was kept under MPPT condition between the periodical $J-V$ measurements).

ITO-coated glass substrates using an rf magnetron sputtering system (SVC-700 RFIINA; Sanyu Electron, Japan). Substrates for devices and glasses for characterizing the structural, optical, electrical, and compositional properties were deposited in the same batch for side-by-side comparisons. All of the substrates were treated with ultraviolet ozone for 20 min and immediately loaded in the deposition chamber. Before deposition, the chamber was evacuated until the pressure inside it becomes <2 × 10^{-3} Pa; then, pure argon gas was introduced at the rate of 20 sccm. Sputter deposition was carried out in an argon gas pressure of 0.5–6.5 Pa and a rf power supply of 50 W. The thickness of the NiO_x films for pressure <3.5 Pa was about 60–70 nm and that for >5.0 Pa was about 40 nm. Commercially available sintered 99.9% pure NiO was used as the target (Kojundo Chemical Laboratory Co. Ltd, Japan). The thicknesses of the NiO_x films were controlled by regulating the deposition time from 20 min to 2 h. All procedures were carried out in room temperature (no intentional heating).

Materials and Characterizations. All chemicals were purchased from commercial suppliers and used as received, unless stated otherwise. Perovskite precursor solutions were prepared by dissolving PbI_2 (Kanto Chemical, 98% purity) in anhydrous *N*, *N*-dimethylformamide (400 mg mL^{-1}), and methylammonium iodide (MAI) and methylammonium chloride (MACl) (Wako Chemicals, battery grade] in ethanol (50 mg mL^{-1}, 19:1 ratio). $PC_{61}BM$ (Sigma-Aldrich, 99% purity) solution (2 wt %) dissolved in anhydrous chlorobenzene was used for coating the electron transport layer. All solutions were filtered through 0.45 μm syringe filters to avoid the risk of particle formation. AZO nanoparticle ink (Nanograde N-21X) was used to prepare the AZO layer. The XRD patterns were collected using an X-ray diffractometer (Rigaku SmartLab, Japan) (Cu Kα radiation, λ = 1.54050 Å). Top-surface and cross-sectional images were taken using a high-resolution scanning electron microscope (Hitachi, S-4800) at a 5 kV accelerating voltage carefully to avoid damage to the samples. XPS (ULVAC-PHI, VersaProbe II, Japan) was used to analyze the elemental composition of the NiO_x films. The UV–vis absorption spectra were recorded on a UV–vis NIR spectrophotometer (Jasco V-7200). The resistivity of the films was measured by a linear four-probe method. The current density–voltage ($J-V$) characteristics (FF, R_s, and R_{sh}) were analyzed by commercial software (SYSTEMHOUSE SUNRISE Corp.), and the incident monochromatic IPCE spectra and EQE were measured using a spectrometer (SM-250IQE; Bunko-keiki, Japan). For stability testing, the encapsulated devices were evaluated under 1 sun illumination (AM1.5G, no UV-light filtering) and MPPT condition using a solar simulator system equipped with a temperature-controlled oven (BIR-50; Bunko-keiki, Japan). A thermocouple was placed near the sample surface to monitor the testing condition. Histograms of 32 cells with NiO_x HTL (70 ± 3 nm) prepared at 3.5 Pa were deduced from the devices, with an area of 0.19 cm^2 defined by an aperture mask.

Device Fabrication. A thin layer (~30 nm) of PEDOT:PSS (Clevios, Al4083) was formed by spin coating at 3000 rpm and subsequently dried at 120 °C for 15 min on a hot plate in ambient air. Sputter-deposited NiO_x and PEDOT:PSS substrates were transferred to a nitrogen-filled glovebox (<1.0 ppm of O_2 and H_2O), inside which the remaining steps were performed. A PbI_2 film was spin-coated at 3000 rpm for 90 s and then a mixture of MAI and MACl was spun onto the PbI_2 layer at 4000 rpm for 90 s for Cl-mediated interdiffusion.[44] Then, to promote crystallization, those as-grown $CH_3NH_3PbI_{3-x}Cl_x$ perovskite films were placed inside a Petri dish with MACl powders on a hot plate at 100 °C for

DOI: 10.1021/acsomega.7b00538
ACS Omega 2017, 2, 2291–2299

MACl treatment.[41] A $PC_{61}BM$ layer was spun onto the perovskite layer at 700 rpm for 60 s, followed by coating with an AZO layer at 3000 rpm for 30 s. The samples were then transferred to the rf magnetron sputtering chamber outside the glovebox for metal contact (silver) deposition. Ag (150 nm) was sputtered at an Ar pressure of 0.15 Pa. The devices were sealed by encapsulation glasses and UV-curable resins (UV RESIN XNR5516Z; Nagase ChemteX, Japan) before measurement under ambient conditions and the stability test.

■ ASSOCIATED CONTENT

Supporting Information

The Supporting Information is available free of charge on the ACS Publications website at DOI: 10.1021/acsomega.7b00538.

Additional details of the photographs and SEM images of the NiO_x films prepared at different Ar pressures of the deposition chamber and the calculation results on the acceleration factors of devices (PDF)

■ AUTHOR INFORMATION

Corresponding Author

*E-mail: SHIRAI.Yasuhiro@nims.go.jp.

ORCID

Yasuhiro Shirai: 0000-0003-2164-5468

Notes

The authors declare no competing financial interest.

■ ACKNOWLEDGMENTS

This study was supported, in part, by the MEXT Program for the Development of Environmental Technology using Nanotechnology, JSPS KAKENHI (grant number JP16K06285), and the Special Doctoral Program for Green Energy Conversion Science and Technology, University of Yamanashi, Japan, through the "Program for Leading Graduates Schools".

■ REFERENCES

(1) Kojima, A.; Teshima, K.; Shirai, Y.; Miyasaka, T. Organometal Halide Perovskites as Visible-Light Sensitizers for Photovoltaic Cells. *J. Am. Chem. Soc.* **2009**, *131*, 6050−6051.

(2) Correa-Baena, J.-P.; Abate, A.; Saliba, M.; Tress, W.; Jesper Jacobsson, T.; Gratzel, M.; Hagfeldt, A. The rapid evolution of highly efficient perovskite solar cells. *Energy Environ. Sci.* **2017**, *10*, 710.

(3) Bi, D.; Tress, W.; Dar, M. I.; Gao, P.; Luo, J.; Renevier, C.; Schenk, K.; Abate, A.; Giordano, F.; Correa Baena, J.-P.; Decoppet, J.-D.; Zakeeruddin, S. M.; Nazeeruddin, M. K.; Gratzel, M.; Hagfeldt, A. Efficient luminescent solar cells based on tailored mixed-cation perovskites. *Sci. Adv.* **2016**, *2*, No. e1501170.

(4) Xu, T.; Chen, L.; Guo, Z.; Ma, T. Strategic improvement of the long-term stability of perovskite materials and perovskite solar cells. *Phys. Chem. Chem. Phys.* **2016**, *18*, 27026−27050.

(5) Aldibaja, F. K.; Badia, L.; Mas-Marza, E.; Sanchez, R. S.; Barea, E. M.; Mora-Sero, I. Effect of different lead precursors on perovskite solar cell performance and stability. *J. Mater. Chem. A* **2015**, *3*, 9194−9200.

(6) Wang, D.; Wright, M.; Elumalai, N. K.; Uddin, A. Stability of perovskite solar cells. *Sol. Energy Mater. Sol. Cells* **2016**, *147*, 255−275.

(7) Chen, W.; Wu, Y.; Yue, Y.; Liu, J.; Zhang, W.; Yang, X.; Chen, H.; Bi, E.; Ashraful, I.; Grätzel, M.; Han, L. Efficient and stable large-area perovskite solar cells with inorganic charge extraction layers. *Science* **2015**, *350*, 944−948.

(8) Bush, K. A.; Bailie, C. D.; Chen, Y.; Bowring, A. R.; Wang, W.; Ma, W.; Leijtens, T.; Moghadam, F.; McGehee, M. D. Thermal and Environmental Stability of Semi-Transparent Perovskite Solar Cells for Tandems Enabled by a Solution-Processed Nanoparticle Buffer Layer and Sputtered ITO Electrode. *Adv. Mater.* **2016**, *28*, 3937−3943.

(9) Saliba, M.; Matsui, T.; Seo, J.-Y.; Domanski, K.; Correa-Baena, J.-P.; Nazeeruddin, M. K.; Zakeeruddin, S. M.; Tress, W.; Abate, A.; Hagfeldt, A.; Grätzel, M. Cesium-containing triple cation perovskite solar cells: improved stability, reproducibility and high efficiency. *Energy Environ. Sci.* **2016**, *9*, 1989−1997.

(10) Burschka, J.; Pellet, N.; Moon, S. J.; Humphry-Baker, R.; Gao, P.; Nazeeruddin, M. K.; Gratzel, M. Sequential deposition as a route to high-performance perovskite-sensitized solar cells. *Nature* **2013**, *499*, 316−319.

(11) Mei, A.; Li, X.; Liu, L. F.; Ku, Z. L.; Liu, T. F.; Rong, Y. G.; Xu, M.; Hu, M.; Chen, J. Z.; Yang, Y.; Gratzel, M.; Han, H. W. A hole-conductor-free, fully printable mesoscopic perovskite solar cell with high stability. *Science* **2014**, *345*, 295−298.

(12) Tsai, H.; Nie, W.; Blancon, J.-C.; Stoumpos, C. C.; Asadpour, R.; Harutyunyan, B.; Neukirch, A. J.; Verduzco, R.; Crochet, J. J.; Tretiak, S.; Pedesseau, L.; Even, J.; Alam, M. A.; Gupta, G.; Lou, J.; Ajayan, P. M.; Bedzyk, M. J.; Kanatzidis, M. G.; Mohite, A. D. High-efficiency two-dimensional Ruddlesden−Popper perovskite solar cells. *Nature* **2016**, *536*, 312−316.

(13) Jong, M. P. d.; IJzendoorn, L. J. v.; Voigt, M. J. A. d. Stability of the interface between indium-tin-oxide and poly(3,4-ethylenedioxythiophene)/poly(styrenesulfonate) in polymer light-emitting diodes. *Appl. Phys. Lett.* **2000**, *77*, 2255−2257.

(14) Huang, A. B.; Zhu, J. T.; Zheng, J. Y.; Yu, Y.; Liu, Y.; Yang, S. W.; Bao, S. H.; Lei, L.; Jin, P. Achieving high-performance planar perovskite solar cells with co-sputtered Co-doping NiOx hole transport layers by efficient extraction and enhanced mobility. *J. Mater. Chem. C* **2016**, *4*, 10839−10846.

(15) Manders, J. R.; Tsang, S. W.; Hartel, M. J.; Lai, T. H.; Chen, S.; Amb, C. M.; Reynolds, J. R.; So, F. Solution-Processed Nickel Oxide Hole Transport Layers in High Efficiency Polymer Photovoltaic Cells. *Adv. Funct. Mater.* **2013**, *23*, 2993−3001.

(16) Park, J. H.; Seo, J.; Park, S.; Shin, S. S.; Kim, Y. C.; Jeon, N. J.; Shin, H. W.; Ahn, T. K.; Noh, J. H.; Yoon, S. C.; Hwang, C. S.; Seok, S. I. Efficient CH3NH3PbI3 Perovskite Solar Cells Employing Nanostructured p-Type NiO Electrode Formed by a Pulsed Laser Deposition. *Adv. Mater.* **2015**, *27*, 4013−4019.

(17) Wang, K. C.; Jeng, J. Y.; Shen, P. S.; Chang, Y. C.; Diau, E. W. G.; Tsai, C. H.; Chao, T. Y.; Hsu, H. C.; Lin, P. Y.; Chen, P.; Guo, T. F.; Wen, T. C. p-type Mesoscopic Nickel Oxide/Organometallic Perovskite Heterojunction Solar Cells. *Sci. Rep.* **2014**, *4*, No. 4756.

(18) Jeng, J. Y.; Chen, K. C.; Chiang, T. Y.; Lin, P. Y.; Tsai, T. D.; Chang, Y. C.; Guo, T. F.; Chen, P.; Wen, T. C.; Hsu, Y. J. Nickel Oxide Electrode Interlayer in CH3NH3PbI3 Perovskite/PCBM Planar-Heterojunction Hybrid Solar Cells. *Adv. Mater.* **2014**, *26*, 4107−4113.

(19) Hu, L.; Peng, J.; Wang, W. W.; Xia, Z.; Yuan, J. Y.; Lu, J. L.; Huang, X. D.; Ma, W. L.; Song, H. B.; Chen, W.; Cheng, Y. B.; Tang, J. Sequential Deposition of CH3NH3PbI3 on Planar NiO Film for Efficient Planar Perovskite Solar Cells. *ACS Photonics* **2014**, *1*, 547−553.

(20) Wang, K. C.; Shen, P. S.; Li, M. H.; Chen, S.; Lin, M. W.; Chen, P.; Guo, T. F. Low-Temperature Sputtered Nickel Oxide Compact Thin Film as Effective Electron Blocking Layer for Mesoscopic NiO/CH3NH3PbI3 Perovskite Heterojunction Solar Cells. *ACS Appl. Mater. Interfaces* **2014**, *6*, 11851−11858.

(21) Zhu, Z. L.; Bai, Y.; Zhang, T.; Liu, Z. K.; Long, X.; Wei, Z. H.; Wang, Z. L.; Zhang, L. X.; Wang, J. N.; Yan, F.; Yang, S. H. High-Performance Hole-Extraction Layer of Sol-Gel-Processed NiO Nanocrystals for Inverted Planar Perovskite Solar Cells. *Angew. Chem., Int. Ed.* **2014**, *53*, 12571−12575.

(22) Chen, W.; Wu, Y.; Liu, J.; Qin, C.; Yang, X.; Islam, A.; Cheng, Y.-B.; Han, L. Hybrid interfacial layer leads to solid performance improvement of inverted perovskite solar cells. *Energy Environ. Sci.* **2015**, *8*, 629−640.

(23) Yin, X. T.; Que, M. D.; Xing, Y. L.; Que, W. X. High efficiency hysteresis-less inverted planar heterojunction perovskite solar cells with a solution-derived NiOx hole contact layer. *J. Mater. Chem. A* **2015**, *3*, 24495−24503.

DOI: 10.1021/acsomega.7b00538
ACS Omega 2017, 2, 2291−2299

(24) Liu, Z. H.; Zhang, M.; Xu, X. B.; Bu, L. L.; Zhang, W. J.; Li, W. H.; Zhao, Z. X.; Wang, M. K.; Cheng, Y. B.; He, H. S. p-Type mesoscopic NiO as an active interfacial layer for carbon counter electrode based perovskite solar cells. *Dalton Trans.* **2015**, *44*, 3967−3973.
(25) Kim, H.-S.; Seo, J.-Y.; Park, N.-G. Impact of Selective Contacts on Long-Term Stability of CH3NH3PbI3 Perovskite Solar Cells. *J. Phys. Chem. C* **2016**, *120*, 27840−27848.
(26) Kim, I. S.; Cao, D. H.; Buchholz, D. B.; Emery, J. D.; Farha, O. K.; Hupp, J. T.; Kanatzidis, M. G.; Martinson, A. B. F. Liquid Water- and Heat-Resistant Hybrid Perovskite Photovoltaics via an Inverted ALD Oxide Electron Extraction Layer Design. *Nano Lett.* **2016**, *16*, 7786−7790.
(27) Zhang, H.; Cheng, J.; Lin, F.; He, H.; Mao, J.; Wong, K. S.; Jen, A. K. Y.; Choy, W. C. H. Pinhole-Free and Surface-Nanostructured NiOx Film by Room-Temperature Solution Process for High-Performance Flexible Perovskite Solar Cells with Good Stability and Reproducibility. *ACS Nano* **2016**, *10*, 1503−1511.
(28) Kwon, U.; Kim, B.-G.; Nguyen, D. C.; Park, J.-H.; Ha, N. Y.; Kim, S.-J.; Ko, S. H.; Lee, S.; Lee, D.; Park, H. J. Solution-Processible Crystalline NiO Nanoparticles for High-Performance Planar Perovskite Photovoltaic Cells. *Sci. Rep.* **2016**, *6*, No. 30759.
(29) You, J.; Meng, L.; Song, T.-B.; Guo, T.-F.; Yang, Y.; Chang, W.-H.; Hong, Z.; Chen, H.; Zhou, H.; Chen, Q.; Liu, Y.; De Marco, N.; Yang, Y. Improved air stability of perovskite solar cells via solution-processed metal oxide transport layers. *Nat. Nanotechnol.* **2016**, *11*, 75−81.
(30) Bai, Y.; Chen, H. N.; Xiao, S.; Xue, Q. F.; Zhang, T.; Zhu, Z. L.; Li, Q.; Hu, C.; Yang, Y.; Hu, Z. C.; Huang, F.; Wong, K. S.; Yip, H. L.; Yang, S. H. Effects of a Molecular Monolayer Modification of NiO Nanocrystal Layer Surfaces on Perovskite Crystallization and Interface Contact toward Faster Hole Extraction and Higher Photovoltaic Performance. *Adv. Funct. Mater.* **2016**, *26*, 2950−2958.
(31) Hou, Y.; Chen, W.; Baran, D.; Stubhan, T.; Luechinger, N. A.; Hartmeier, B.; Richter, M.; Min, J.; Chen, S.; Quiroz, C. O. R.; Li, N.; Zhang, H.; Heumueller, T.; Matt, G. J.; Osvet, A.; Forberich, K.; Zhang, Z. G.; Li, Y. F.; Winter, B.; Schweizer, P.; Spiecker, E.; Brabec, C. J. Overcoming the Interface Losses in Planar Heterojunction Perovskite-Based Solar Cells. *Adv. Mater.* **2016**, *28*, 5112−5120.
(32) Mali, S. S.; Kim, H.; Shim, S. E.; Hong, C. K. A solution processed nanostructured p-type NiO electrode for efficient inverted perovskite solar cells. *Nanoscale* **2016**, *8*, 19189−19194.
(33) Guo, D.; Yu, J.; Fan, K.; Zou, H.; He, B. Nanosheet-based printable perovskite solar cells. *Sol. Energy Mater. Sol. Cells* **2017**, *159*, 518−525.
(34) Ciro, J.; Betancur, R.; Mesa, S.; Jaramillo, F. High performance perovskite solar cells fabricated under high relative humidity conditions. *Sol. Energy Mater. Sol. Cells* **2017**, *163*, 38−42.
(35) Yin, X. T.; Chen, P.; Que, M. D.; Xing, Y. L.; Que, W. X.; Niu, C. M.; Shao, J. Y. Highly Efficient Flexible Perovskite Solar Cells Using Solution-Derived NiOx Hole Contacts. *ACS Nano* **2016**, *10*, 3630−3636.
(36) Yin, X.; Liu, J.; Ma, J.; Zhang, C.; Chen, P.; Que, M.; Yang, Y.; Que, W.; Niu, C.; Shao, J. Solvothermal derived crystalline NiOx nanoparticles for high performance perovskite solar cells. *J. Power Sources* **2016**, *329*, 398−405.
(37) Patnaik, P. *Handbook of Inorganic Chemicals*; McGraw-Hill: New York, 2003.
(38) Nandy, S.; Saha, B.; Mitra, M. K.; Chattopadhyay, K. K. Effect of oxygen partial pressure on the electrical and optical properties of highly (200) oriented p-type Ni1-xO films by DC sputtering. *J. Mater. Sci.* **2007**, *42*, 5766−5772.
(39) Chen, H. L.; Yang, Y. S. Effect of crystallographic orientations on electrical properties of sputter-deposited nickel oxide thin films. *Thin Solid Films* **2008**, *516*, 5590−5596.
(40) Kim, H. S.; Jang, I. H.; Ahn, N.; Choi, M.; Guerrero, A.; Bisquert, J.; Park, N. G. Control of I−V Hysteresis in CH3NH3PbI3 Perovskite Solar Cell. *J. Phys. Chem. Lett.* **2015**, *6*, 4633−4639.
(41) Khadka, D. B.; Shirai, Y.; Yanagida, M.; Masuda, T.; Miyano, K. Enhancement in efficiency and optoelectronic quality of perovskite thin films annealed in MACl vapor. *Sustainable Energy Fuels* **2017**, *131*, 6050.
(42) De Bastiani, M.; Dell'Erba, G.; Gandini, M.; D'Innocenzo, V.; Neutzner, S.; Kandada, A. R. S.; Grancini, G.; Binda, M.; Prato, M.; Ball, J. M.; Caironi, M.; Petrozza, A. Ion Migration and the Role of Preconditioning Cycles in the Stabilization of the J−V Characteristics of Inverted Hybrid Perovskite Solar Cells. *Adv. Energy Mater.* **2016**, *6*, No. 1501453.
(43) Schuller, S.; Schilinsky, P.; Hauch, J.; Brabec, C. J. Determination of the degradation constant of bulk heterojunction solar cells by accelerated lifetime measurements. *Appl. Phys. A: Mater. Sci. Process.* **2004**, *79*, 37−40.
(44) Tripathi, N.; Yanagida, M.; Shirai, Y.; Masuda, T.; Han, L.; Miyano, K. Hysteresis-free and highly stable perovskite solar cells produced via a chlorine-mediated interdiffusion method. *J. Mater. Chem. A* **2015**, *3*, 12081−12088.

DOI: 10.1021/acsomega.7b00538
ACS Omega 2017, 2, 2291−2299